High-resolution 3D seismic imaging and refined velocity model building improve the image of a deep geothermal reservoir in the Upper Rhine Graben

Nicolas Salaun[1], Helene Toubiana[1], Jean-Baptiste Mitschler[1], Guillaume Gigou[1], Xavier Carriere[1], Vincent Maurer[2], and Alexandre Richard[2]

https://doi.org/10.1190/tle39120857.1

Abstract

Over the past 35 years, geothermal projects have been developed in the Upper Rhine Graben (URG) to exploit deep geothermal energy. Underneath approximately 2 km of sedimentary deposits, the deep target consists of a granitic basement, which is highly fractured and hydrothermally altered. Therefore, it has high potential as a geothermal reservoir. Despite dense 2D seismic data coverage originally acquired for oil exploration (for a target two-way traveltime between 300 and 700 ms), the faults at the top of the granitic basement (between 1400 and 4000 ms) are poorly imaged, and their locations remain uncertain. To gain a better understanding of this large-scale faulting and to ensure the viability of future geothermal projects, a 3D seismic survey was acquired in the French part of the URG during the summer of 2018. This paper describes how an integrated project, combining seismic data processing, high-end imaging, and enhanced interpretation, was conducted to improve the understanding of this complex basin for geothermal purposes. By revealing the deep granite layer and its complex associated fault network, the insight from this project can help accurately locate future production wells.

Introduction

The Upper Rhine Graben (URG), with deep-seated fault systems, is well known for its high geothermal potential (Dornstädter et al., 1999; Kreuter et al., 2003). The area is characterized by several local thermal anomalies associated with hydrothermal convective cells. These cells are circulating inside a nearly vertical fracture network in the granitic basement and the Triassic fractured sediments above it (Pribnow and Clauser, 2000). Many geothermal projects are operational in the URG, including Landau, Insheim, and Bruchsal in Germany and Soultz-sous-Forêts and Rittershoffen in France (Vidal and Genter, 2018). Moreover, new geothermal projects are in the exploration phase of deep drilling in the Strasbourg area (Boissavy et al., 2019). The geothermal targets are primarily the granitic basement and its sedimentary cover represented by Permo-Triassic sandstones, both of which are highly fractured. Generally, highly dipping normal faults related to the URG's tectonic history bear geothermal brines (Bächler et al., 2003). The brines are exploited for producing either electricity, as at Soultz, or heat at high temperatures, as at Rittershoffen (Baujard et al., 2018). In the latter case, since 2016, this industrial site has been producing 24 MW of geothermal heat from a high-temperature (greater than 160°C) well for a biorefinery with consistent availability of power.

To understand fluid migration and heat transport, geothermal engineers wish to identify the location of impermeable sealed faults in order to optimize their well drilling plans. As geothermal energy use involves pumping out hot water and reinjecting cold water, it is crucial for its sustainability that hot and cold water do not mix in the subsurface. Accurately imaging the fault network is key to understanding potential fault connections and selecting the best places to drill. Advanced seismic reflection imaging is currently the best method for providing high-resolution imaging of such complex geologic systems, as demonstrated by Louie et al. (2012). The successful appraisal and development of geothermal heat requires a deep understanding of the subsurface environment. The oil and gas industry has experience and expertise in characterizing deep and ultradeep formations. This can be successfully transferred to develop and apply solutions for exploring, mapping, and producing geothermal resources (Sosio et al., 2019).

In the URG, the altered granitic basement is located below 2 km of structured sediment layers and suffers from a poor signal-to-noise ratio (S/N) for seismic imaging. This, coupled with complex raypaths generated by the overburden, plays a part in concealing target faults in vintage seismic images. The seismic data available in this region were acquired many years ago for oil and gas exploration and are not well suited to geothermal exploration due to a lack of emitted low frequencies (acquisition source sweeps had a lower limit of 10 Hz) (Durst, 1991). Moreover, most of the seismic acquisitions were 2D. Eichkitz et al. (2009) have shown the importance of using 3D seismic data to increase the reliability of the model.

To extend its geothermal activity in the region, Électricité de Strasbourg acquired a dedicated 3D wide-azimuth seismic survey over Northern Alsace in 2018 (Figure 1) (Richard et al., 2019). Following data acquisition, seismic processing and high-end imaging were conducted in 2019 to characterize the deep faulted structures and ensure high-resolution imaging of shallower parts of the section. An iterative processing flow was implemented and a 3D migration was performed as a standard QC measure to evaluate the results and potentially modify the interpretation. This close interaction between teams of geologists and geophysicists provided greater confidence in the selected

[1]CGG, Massy, France. E-mail: nicolas.salaun@cgg.com; toubiana.helene@cgg.com; jean-baptiste.mitschler@cgg.com; guillaume.gigou@cgg.com; xavier.carriere@cgg.com.
[2]Électricité de Strasbourg, Schiltigheim, France. E-mail: vincent.maurer@es.fr; alexandre.richard@es.fr.

processing parameters and was highly beneficial for velocity model building and imaging.

The first section of this paper describes the technology used to reconstruct the shallow surface information and to correct for the weathering zone (WZ) distortion and noise effects. The second section describes the velocity model building flow used to obtain an accurate subsurface image and to reveal the fault definition. The last section describes and further discusses interpretation of the fault network and the understanding of fluid transfer.

Sparse shallow subsurface sampling

The benefits of the very low frequencies recorded during the 2018 acquisition (source sweep of 2 to 96 Hz recorded by geophone SG-10) can be clearly seen in Figure 2. The new image reveals several key features including basement top (corresponding to altered granite), potentially the base of the altered granite, and deep target faults. Crucial for target imaging, emitted low-frequency energy mainly propagates as surface waves, therefore concealing the recorded reflection wave used for imaging. Although elastic waves are usually compensated for by a specific receiver array design, this was not done here due to operational constraints. The survey was acquired during harvest season, and it was crucial to minimize crew movement. For this reason, a shot-blending approach was implemented to speed up acquisition and to optimize productivity (Meunier and Bianchi, 2005). To facilitate sensor layout in the field, bunched strings of geophones were sometimes used rather than receiver arrays. These two factors plus the moderate fold (150) led to a relatively high level of noise that the seismic processing had to overcome in order to recover the full value of the modern survey data.

As surface waves were not filtered by the acquisition design, they had to be modeled and removed during preprocessing to significantly reduce the noise level in the low frequencies. First, the distortion effects due to elevation and near-surface waves had to be resolved. The surface area is largely covered by corn fields and forest. The topography of the area is relatively flat, so it does not pose any specific problems for seismic imaging. Its WZ, however, generates very slow P-wave velocities, with some areas as slow as 250 m/s^{-1} and with a large thickness variation ranging from 0 to 40 m. To build a multilayer geologic model of the WZ, seismic refraction and uphole surveys were carried out. A near-surface geologic model, containing layers varying in both velocity and thickness, was used

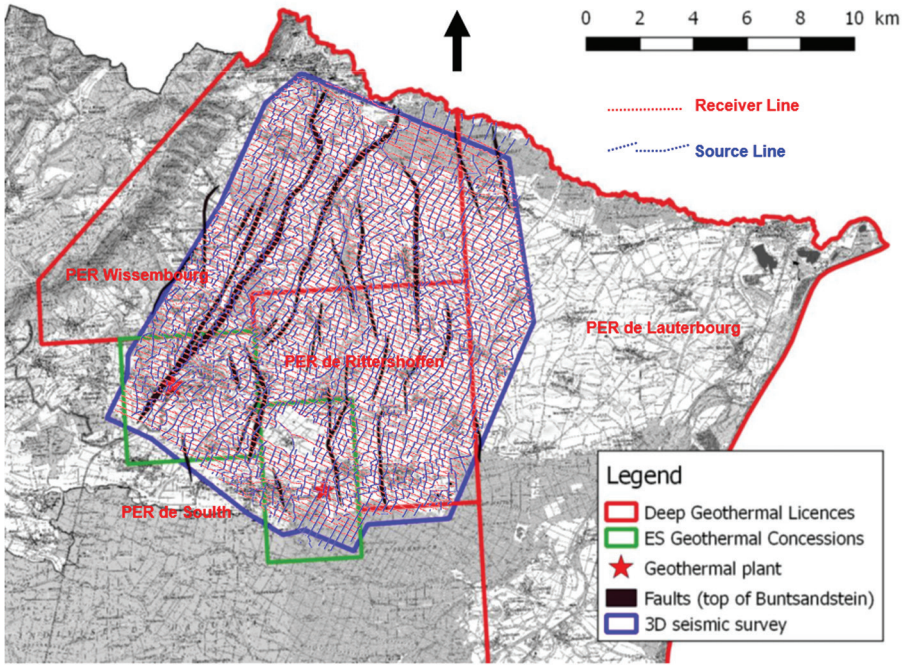

Figure 1. Map showing the location of the 180 km^2 of 3D seismic acquired in Northern Alsace, France, in 2018.

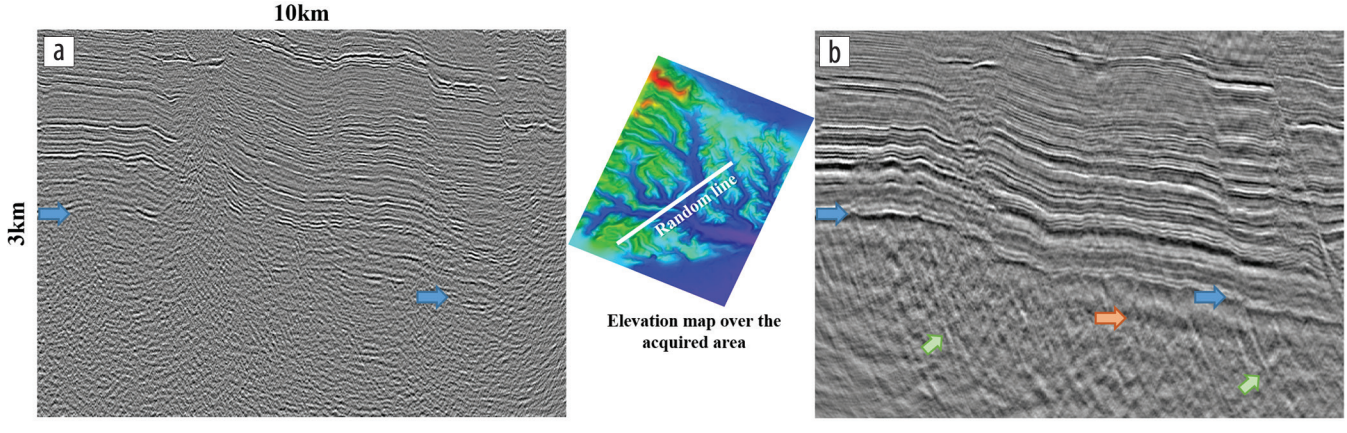

Figure 2. (a) A vintage 2D section compared with (b) a random line from the 2019 final 3D volume. The additional low-frequency information helps delineate sediment lithology and fully reveals the Permian event (blue arrows) followed by the fractured granite. This altered granite can now be tracked along the full area. Target faults inside the granite layer (green arrows) are also clearly visible and interpretable. The orange arrow highlights the base of the granite, which is trackable on a part of the survey.

to derive static corrections. The corrections were applied prior to the main preprocessing and imaging flows. Although the model was calibrated where upholes were available, the lack of near-offset primary reflections needed to image the shallow subsurface made it difficult for us to assess our geologic model away from the well control points. This issue was mitigated by using information from the multiple reflections bouncing between the recording surface and the strong contrast at the WZ base. This information was extracted via shot and receiver deconvolution operators (Retailleau, 2015). The high source density of the acquisition enabled the construction of finely sampled 3D near-surface volumes. The broadband sweep (without side lobes) was conducive to provide clean operators in which reflections could be extracted up to very shallow depths. With the reconstructed shallow surface layer, we were able to better model the velocities and QC the reliability of the WZ (Figures 3a–3c). The resulting high-resolution image is of significant value to define further well locations and to avoid shallow drilling hazards such as a shallow active fault.

Time static corrections derived from the geologic model, varying in thickness and velocity, were used to compensate for the low-frequency distortion implied by the shallow surface. After correction, reflection events were more continuous as were surface waves, which also suffered from the distortion of the uncorrected WZ perturbation.

Prior to the start of ground-roll model building, an additional step was required. This was because the slow velocities of the shallow layers, coupled with the relatively sparse receiver grid in the acquisition design (200 × 40 m), led to heavily aliased surface-wave energy (Figure 4a). Dealiasing of the surface waves was critical to enable us to model and remove this unwanted seismic energy. To achieve this, we performed trace densification to increase the spatial sampling, interpolating by a factor of 4 along both the receiver and source lines using a combined low-rank and sparse inversion (Sternfels et al., 2016). Because surface-wave velocities varied over the survey location and were dispersive, different velocities had to be used for each frequency. Figure 4b shows a dense cross-spread after the interpolation, highlighting the dealiased surface waves.

Using the densely sampled data, we applied a data-driven interferometry method to produce an accurate low-frequency model of the ground roll (Chiffot et al., 2017). This model was 3D adaptively subtracted from the data to produce a data set free of ground roll (Figure 5). The adaptive subtraction compensated for kinematic inaccuracies in the model and better separated strong organized noise from primary energy, especially diffraction noise, which is crucial to properly image the faults.

After ground-roll attenuation and in addition to this random noise attenuation, a final improvement in S/N was achieved by preimaging trace densification. The source and receiver lines were each interpolated by a factor of 2, resulting in a fold increase from 150 to 600. This interpolation was performed in the 5D domain, coupled with regularization in order to obtain an ideal acquisition geometry map (Wang and Wang, 2013). Having five dimensions to work with enables better filling of large gaps and ensures homogenized coverage for each offset/azimuth sector, which is important for subsequent fracture analysis. Trace densification also improves the near-offset coverage, enhancing the quality of

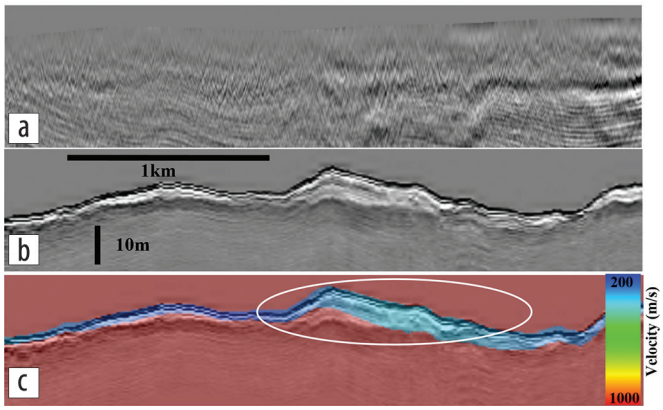

Figure 3. (a) Time-migrated seismic section, with datuming from topography to final datum, as recorded. (b) Shallow layer reconstructed using deconvolution operators stretched back to depth with the geologic model velocity. (c) Shallow layer reconstructed using deconvolution operators stretched back to depth with the velocity model below the acquisition surface down to the WZ base.

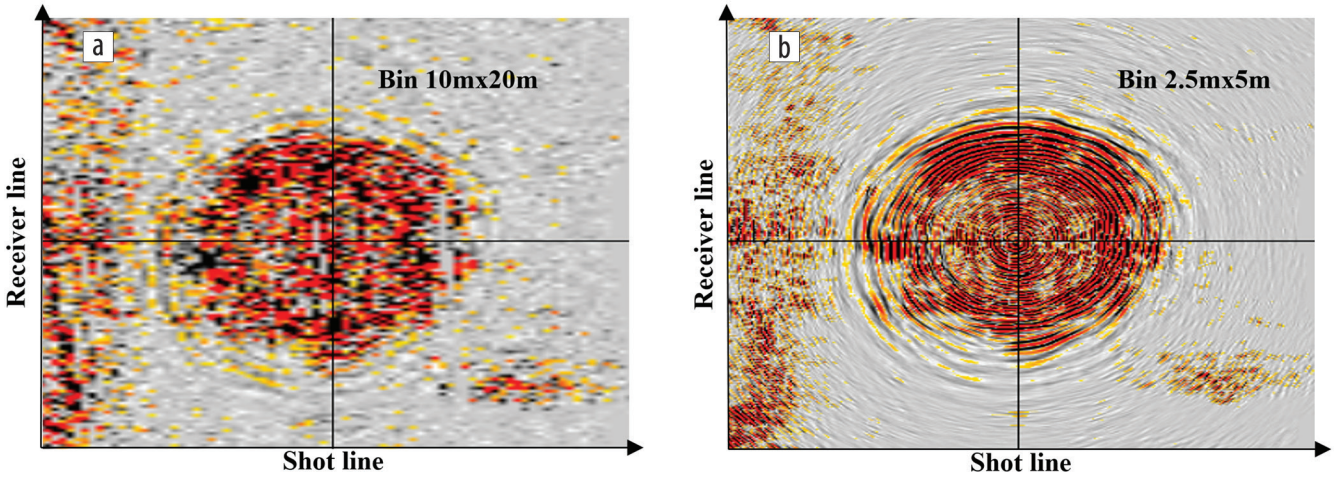

Figure 4. (a) Time slice cutting through a raw cross-spread. Ground-roll noise is clearly visible but is not continuous due to aliasing. This makes it difficult to model. After the densification in (b), aliasing is no longer present, and events are more coherent.

near-surface imaging. This last point was important during velocity model building as it helped calibrate shallow reflectors with well information.

Fault-oriented velocity model building and least-squares imaging

During the preprocessing flow, each step was validated by migrating the full 3D volume in order to assess imaging quality of the deep faulting. These volumes were delivered to interpreters, ensuring regular feedback. A 3D structural model (Figure 6a) was used both as a QC and as a guide for the imaging team and was iteratively built from picked faults and key horizons on delivered volumes (Figure 6b). The ultimate goal of the structural model was to locate future production wells so that they cross the main faults to drain hot water. To refine fault definition and location, fault-oriented velocity model building was performed, using and refining interpreted information to guide the work.

The first step of the velocity model building involved updating the shallow subsurface layers where, as discussed in the previous section, the lack of near offset in the acquisition did not permit reflection energy to be recorded. While the near-surface geologic model and derived static corrections handled the first few tens of meters of depth, this part aimed to update velocity in the first few hundred meters. For this, the velocity update relied on refracted P-wave energy. After picking first arrivals for each shotpoint, a first-break tomography process was used to compute a near-surface velocity model.

Based on the velocity update for the shallow layers, a velocity update for the deeper part of the section was estimated using multilayer tomography (Guillaume et al., 2012). This tomographic workflow enables each layer to be parameterized independently and helps to produce a more accurate result, especially in the presence of sharp velocity contrasts. Geologic horizons, interpreted from the 3D structural model, were used to constrain the update of the velocity field. In this project, three horizons were defined corresponding to strong velocity contrasts. We used well ties and velocity trends to QC the velocity updates along with regional well information such as well tops, facies interfaces, and sonic logs.

During the inversion, we used a fault-constrained update to overcome lateral smoothing across faults where large velocity variations may exist. For this purpose, the main fault planes in the structural model were input to the tomography, in addition to the earlier-described horizons. Introduction of this contrast in the velocity field for the prestack depth migration (PSDM) improved flattening of events on either side of each fault and produced sharper imaging of the fault planes. For the granitic basement velocity, we carried out scans, along with well information where available. However, as previous wells were drilled for oil exploration purposes (shallower targets between 300 and 700 ms), only one well penetrated deep enough to provide access to the granitic basement velocity. Throughout the

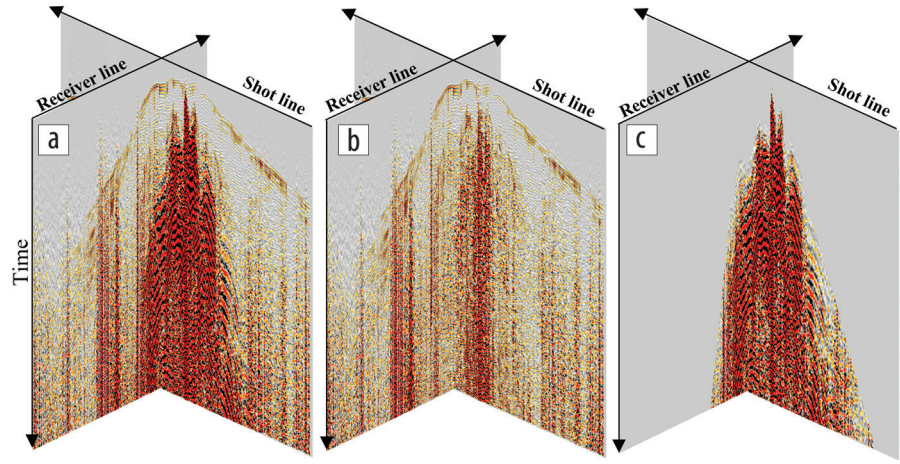

Figure 5. (a) Cross-spread (in original geometry) with visible complex surface waves. (b) The same cross-spread after removal of the surface waves. (c) Attenuated energy. This step is important to recover the low-frequency signal needed for deep imaging.

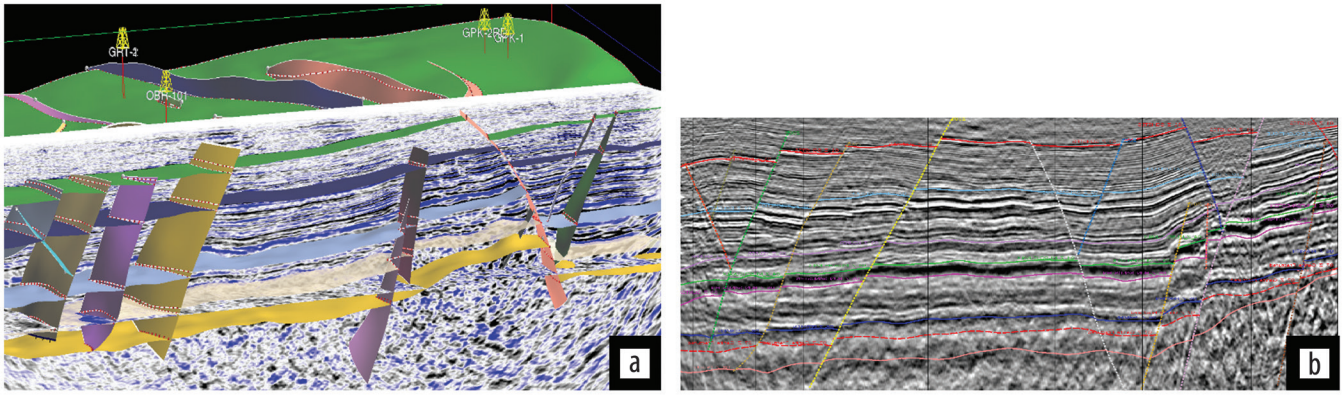

Figure 6. (a) Three-dimensional structural model containing wells, horizons, and fault planes iteratively built from (b) various interpreted seismic volumes delivered after different steps of preprocessing and imaging. The model was also used to refine the velocity model in order to locate future production wells. The dark blue line shows the Permian horizon. The red line shows the fractured granite.

earlier-described flow, anisotropy was carefully refined to tie wells and ensure delivery of a calibrated seismic image with a reliable layer thickness. The updated velocity model was then used for final imaging. Inclusion of fault interpretation in the tomography enabled improved imaging of the fault planes, easing its tracking on the depth slice. However, noise from the migration response still remained locally.

All of the preprocessing, denoising, amplitude compensation, and regularization steps were designed to provide the best imaging of the deep fault network present in the granitic layer. However, residual noise, the complex velocity model, and imperfect acquisition design caused visible migration artifacts. These artifacts were the result of imbalanced illumination. To improve fault interpretation, we performed Kirchhoff least-squares PSDM (LS-PSDM). As described by Guitton (2004), this method aims to correct for migration artifacts that result from an incomplete description of the wave propagation and irregularities in the input data. Figure 7 shows reasonable attenuation of migration artifacts with improved imaging of the underlying structure. This noise attenuation also reinforced real fault energy, further enhancing interpretation. The final volume accurately imaged the complex geologic structure and, after calibration in depth, was used for final interpretation work.

Geothermal reservoir interpretation

Before the 2018 acquisition and 2019 processing of 3D data, geologic interpretation of large parts of the French URG was performed using only 2D seismic sections. In addition to poor imaging of the altered granite layer and its associated factures, this information was sparsely distributed over the area. Having access to a 3D volume enabled confirmation and expansion of the vintage interpretation. It also led to a step change in our understanding of the geologic history of the deep URG for further development of geothermal activity in the area.

The structural model, iteratively built and used to improve velocity model building, was updated using the final seismic volume. Besides fault and horizon picking on the seismic image, additional products such as advanced fault enhancement (AFE) were generated and used to better refine the complex fault network interpretation (Figure 8). The AFE volume was derived from a coherence cube and greatly helped with fault picking and imaging (Dorn, 2019). The dedicated processing sequence also enabled derivation of robust

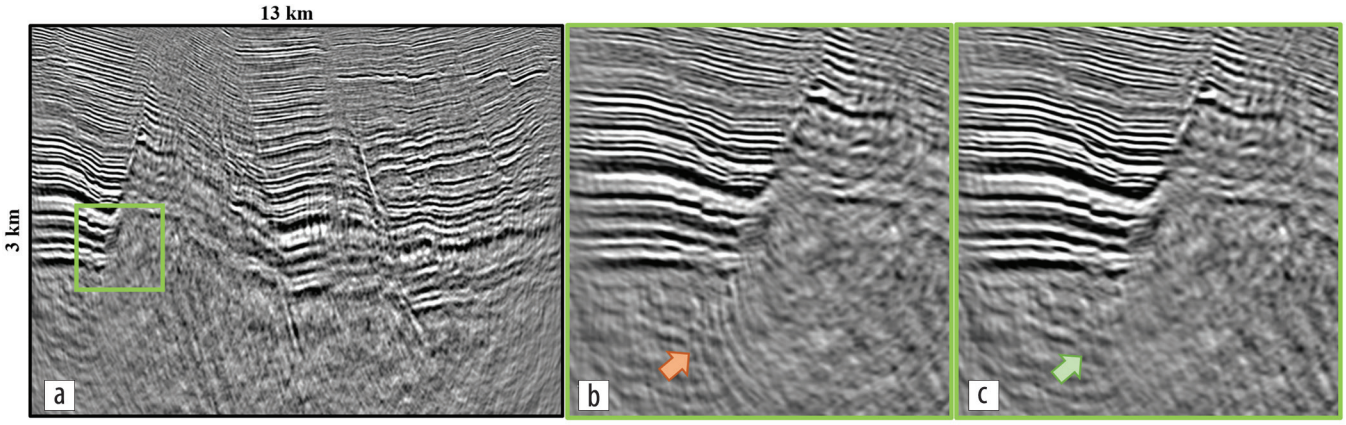

Figure 7. (a) Full-section LS-PSDM stack and close-up of the migration artifact. (b) PSDM versus (c) LS-PSDM. LS-PSDM made it possible to distinguish the fault from the background noise. It showed an uplift in the deeper fault definition. The orange arrow highlights the migration operator noise, which is well attenuated because LS-PSDM provides cleaner results underneath the geologic event (green arrow).

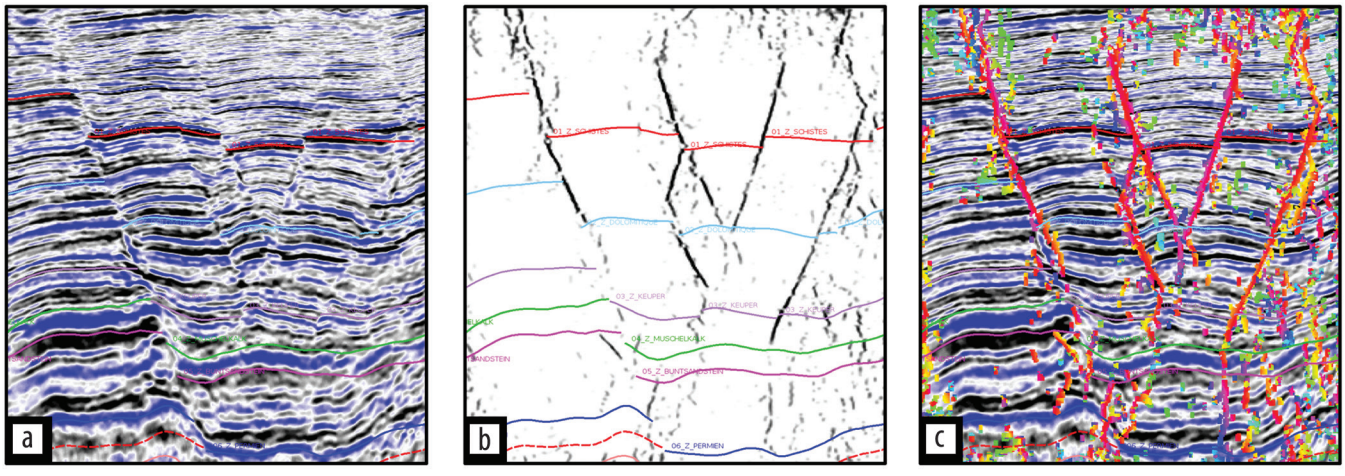

Figure 8. (a) Seismic cross section and interpreted horizon. (b) To ease fault picking, AFE was carried out. (c) Overlaying AFE on the seismic section shows good correlation of this additional product.

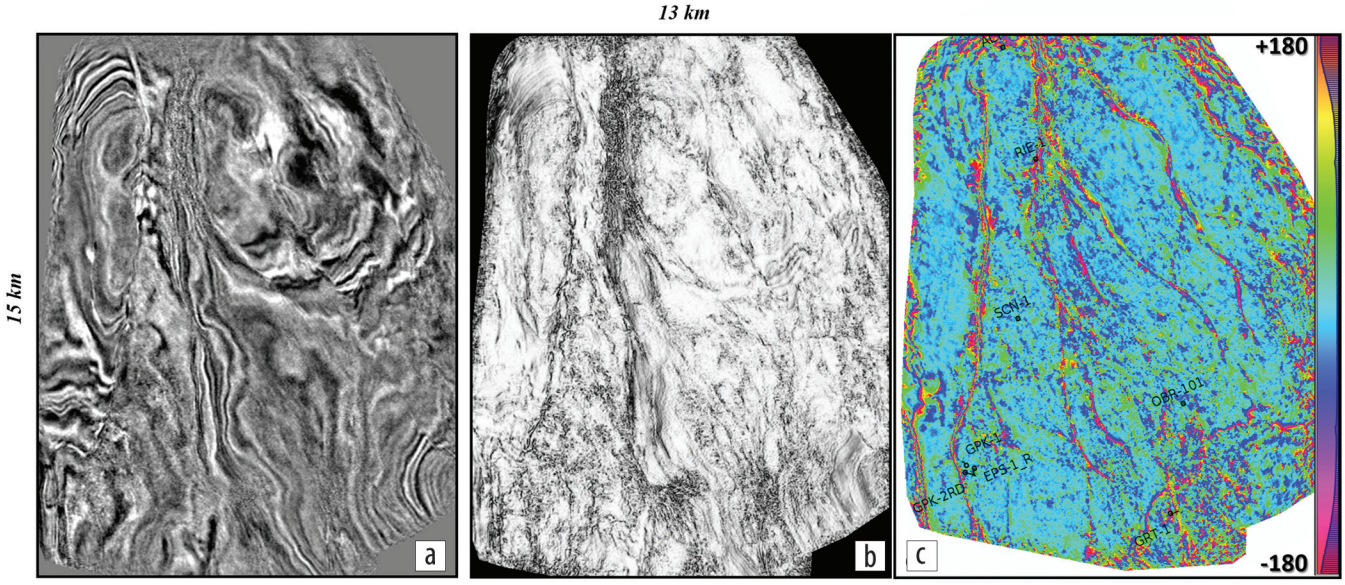

Figure 9. (a) Depth seismic slice compared with (b) the coherency map and (c) instantaneous phase attribute. (b) and (c) highlight fault continuity, making it easier to follow. They ease interpretation of the complex fault network at the top of the granite level.

seismic attributes, such as instantaneous phase, which is particularly suited to highlight event discontinuity. This attribute made it possible to highlight, for the first time in the French URG, an important fault network inside the granite basement on the seismic data. Final interpretation of the fault characterization was achieved through azimuth and dip volumes, leading to a better understanding of fluid transfer inside the deep basement. Structural coherency of the interpretation was built with well-tie constraints and client interaction to ensure its robustness. The ability to display a depth section and attribute maps (Figure 9) of the full area also led to important information on the organization of the main faults. This was particularly important for the Permian layer, located just above the top granite, which is poorly characterized in the vintage 2D lines.

Conclusion

A seismic acquisition survey was conducted over the French URG in 2018 by Electricité de Strasbourg, aiming to fully image the deep granitic basement and its associated fault network. Its deep target design and very low velocities of the shallow subsurface posed particular challenges for subsequent data imaging. The use of information contained in the multiple energy as well as surface-wave densification helped resolve these difficulties. First-break-, multilayer-, and fault-constrained tomography were required to deliver a velocity field, ensuring a high-fidelity migrated image and minimizing mis-ties with the wells. Throughout processing, multiple 3D migrations were performed for QC purposes in order to ensure delivery of accurate images of the deep part of the URG structure. The final volume showed considerable improvement over vintage images and led to building an accurate complex 3D structural model. Additional extracted seismic attributes made it possible to map an important fault network inside the granite basement on the seismic data. The fault network was visible for the first time, providing great benefits to better understand the geologic history and geothermal cycle. This new information will also help locate and define trajectories of future production wells with more confidence. In this rich geothermal region, with strong activity on both sides of the French/German border, the benefits of such imaging could help develop new areas of interest.

In addition to electricity and heat production, the URG deep geothermal reservoir is known as a valuable source of lithium (Pauwels et al., 1990). Recent studies have shown the potential of lithium extraction with a very low environmental impact parallel with geothermal production. This demonstrates growing interest in further exploiting the URG subsurface. TLE

Data and materials availability

Data associated with this research are confidential and cannot be released.

Corresponding author: nicolas.salaun@cgg.com

References

Bächler, D., T. Kohl, and L. Rybach, 2003, Impact of graben-parallel faults on hydrothermal convection — Rhine Graben case study: Physics and Chemistry of the Earth, **28**, no. 9–11, 431–441, https://doi.org/10.1016/S1474-7065(03)00063-9.

Baujard, C., A. Genter, N. Cuenot, J. Mouchot, V. Maurer, R. Hehn, G. Ravier, O. Seibel, and J. Vidal, 2018, Experience from a successful soft stimulation and operational feedback after two years of geothermal power and heat production in Rittershoffen and Soultz-sous-Forêts plants (Alsace, France): Geothermal Resource Council.

Boissavy, C., L. Henry, A. Genter, A. Pomart, P. Rocher, and V. Schmidlé-Bloch, 2019, Geothermal energy use, country update for France: European Geothermal Congress.

Chiffot, C., A. Prescott, M. Grimshaw, F. Oggioni, M. Kowalczyk-Kedzierska, S. Cooper, D. Le Meur, and R. Johnston, 2017, Data-driven interferometry method to remove spatially aliased and nonlinear surface waves: 87th Annual International Meeting, SEG, Expanded Abstracts, 4980–4985, https://doi.org/10.1190/segam2017-17724305.1.

Dorn, G. A., 2019, 3D fault imaging using windowed Radon transforms: An example from the North Sea: First Break, **37**, no. 5, 81–88, https://doi.org/10.3997/1365-2397.n0024.

Dornstadter, J., O. Kappelmeyer, and M. Welter, 1999, The geothermal potential in the Upper Rhine Graben Valley: Presented at the European Geothermal Conference.

Durst, H., 1991, Aspects of exploration history and structural style in the Rhine Graben area: Generation, accumulation and production of Europe's hydrocarbons: European Association of Petroleum Geoscientists.

Eichkitz, C., M. Schreilechner, A. Scholz, U. Lotz, and G. Greiner, 2009, Upper Rhine Graben: 3D seismic — A new approach to geothermal exploration in a structurally complex tectonic environment: 71st Conference and Exhibition, EAGE, Extended Abstracts, https://doi.org/10.3997/2214-4609.201400335.

Guillaume, P., S. Hollingworth, X. Zhang, A. Prescott, R. Jupp, G. Lambaré, and O. Pape, 2012, Multi-layer tomography and its application for improved depth imaging: 82nd Annual International Meeting, SEG, Expanded Abstracts, https://doi.org/10.1190/segam2012-0683.1.

Guitton, A., 2004, Amplitude and kinematic corrections of migrated images for nonunitary imaging operators: Geophysics, **69**, no. 4, 1017–1024, https://doi.org/10.1190/1.1778244.

Kreuter, H., N. Harthill, M. Judt, and B. Lehmann, 2003, Geothermal power generation in the Upper Rhine Valley — The project Offenbach/Pfalz: Presented at the International Geothermal Conference.

Louie, J. N., S. K. Pullammanappallil, and W. Honjas, 2012, Advanced seismic imaging for geothermal development: 82nd Annual International Meeting, SEG, Expanded Abstracts, https://doi.org/10.1190/segam2012-0965.1.

Meunier, J., and T. Bianchi, 2005, Cost-effective, high-density vibroseis acquisition: 75th Annual International Meeting, SEG, Expanded Abstracts, 44–47, https://doi.org/10.1190/1.2142239.

Pauwels, H., M. Brach, and C. Fouillac, 1990, Lithium recovery from geothermal waters of Cesano and Cronenbourg: Presented at the 12th New Zealand Geothermal Workshop.

Pribnow, D., and C. Clauser, 2000, Heat and fluid flow at the Soultz hot dry rock system in the Rhine Graben: Presented at the World Geothermal Congress.

Retailleau, M., 2015, Imaging the near surface using surface-consistent prediction operators — Examples from the Middle East: 77th Conference and Exhibition, EAGE, Extended Abstracts, https://doi.org/10.3997/2214-4609.201413320.

Richard, A., É. Gillot, V. Maurer, N. Cuenot, and J. Klee, 2019, Upper Rhine Graben: The largest geothermal exploration by 3D seismic reflection: Presented at the European Geothermal Congress.

Sosio, G., A. Campana, R. Braham, C. Spyrou, O. Burachok, A. Mandiuc, C. Baujard, and A. Genter, 2019, Mitigating risk in geothermal projects with an integrated modelling approach: A case study in France: First Break, **37**, no. 7, 71–79, https://doi.org/10.3997/1365-2397.n0042.

Sternfels, R., A. Prescott, G. Pignot, L. Tian, and D. Le Meur, 2016, Irregular spatial sampling and rank-reduction — Interpolation by joint low-rank and sparse inversion: 78th Conference and Exhibition, EAGE, Extended Abstracts, https://doi.org/10.3997/2214-4609.201601236.

Vidal, J., and A. Genter, 2018, Overview of naturally permeable fractured reservoirs in the central and southern Upper Rhine Graben: Insights from geothermal wells: Geothermics, **74**, 57–73, https://doi.org/10.1016/j.geothermics.2018.02.003.

Wang, J., and S. Wang, 2013, Hybrid 5D Fourier transform — A flexible tool for land data interpolation: 83rd Annual International Meeting, SEG, Expanded Abstracts, 3603–3607, https://doi.org/10.1190/segam2013-0388.1.